

1100. 8-10 March 1993, pp. 147-152

Sensor and Simulation Notes

Note 277

October 1982

Review of Hybrid and Equivalent-Electric-Dipole
EMP Simulators

Carl E. Baum
Air Force Weapons Laboratory

Abstract

This paper summarizes the design principles for two important classes of simulators for the high-altitude nuclear electromagnetic pulse (EMP). First there is the equivalent electric dipole in the form of a resistively loaded cone on a ground plane; this is appropriate for radiating an optimum pulse to distances large compared to the simulator; it can also expose systems on the ground to a vertically polarized electric field. Second there is a hybrid EMP simulator which is appropriate for producing an approximate plane wave incident on systems on the ground surface together with the ground wave. The characteristics of these two types of simulators are summarized and the basic design equations are summarized.

Approved for public release;
distribution unlimited.

CLEARED FOR PUBLIC RELEASE

AFCMD/PA, 82-368

27 Oct 82

Sensor and Simulation Notes

Note 277

October 1982

Review of Hybrid and Equivalent-Electric-Dipole
EMP Simulators

Carl E. Baum
Air Force Weapons Laboratory

Abstract

This paper summarizes the design principles for two important classes of simulators for the high-altitude nuclear electromagnetic pulse (EMP). First there is the equivalent electric dipole in the form of a resistively loaded cone on a ground plane; this is appropriate for radiating an optimum pulse to distances large compared to the simulator; it can also expose systems on the ground to a vertically polarized electric field. Second there is a hybrid type of EMP simulator which is appropriate for producing an approximate plane wave incident on systems on the ground surface together with the ground reflected wave. The characteristics of these two types of simulators are reviewed and the basic design equations are summarized.

electromagnetic pulse simulators, high altitude, electric fields, plane waves, ground waves.

Approved for public release;
distribution unlimited.

I. Introduction

EMP simulation is now a rather mature discipline. A serious study of this field began almost two decades ago with the publication of the early Sensor and Simulation Notes. Included in the Joint Special Issue on the Nuclear Electromagnetic Pulse published in 1978 is an extensive review (with a large bibliography) of EMP simulation [15]. As noted there, concepts for EMP simulation depend on the location of both the nuclear detonation and the observer; this leads to many different types of EMP simulators. The scope of the present paper is more modest.

Section 2 of [15] considers "Simulators for EMP Outside of Nuclear Source Regions." This is primarily concerned with the high-altitude EMP, in which an exoatmospheric nuclear detonation generates the EMP in a roughly 20-40 km altitude source region, producing an EMP which illuminates both in-flight and ground-based systems over a very wide ground coverage area.

There are various possible high-altitude EMP simulation schemes. Limiting our discussion to cases of high level (threat level or as high a level as reasonably practical) transient electromagnetic fields illuminating reasonably sized systems (excluding, for example, large distributed systems such as power and communication grids) there are currently three popular types of EMP simulators for this kind of high-altitude EMP. For in-flight systems such as missiles and aircraft (excluding trailing-wire antennas) the appropriate type of simulator is of the guided-wave type which is usually realized as a parallel-plate structure for efficiency. This type of simulator is appropriate for producing a single plane wave over a restricted region of space (the working volume). This type of EMP simulator is discussed in a companion paper. This paper considers the other two popular types of high-altitude EMP simulator.

In some cases the system to be tested is extremely large making it difficult to be fitted "inside" an EMP simulator. In other cases one would like the system to be "flying" in its true operational environment, and may be willing to accept, at least for some tests, the reduction of the EMP excitation inherent in the comparatively large distances from the simulator to the system of interest. This leads to a quite different type of EMP simulator which can be characterized (at least for the lower frequencies of interest) as an equivalent dipole (electric in practice).

An important case of interest concerns systems at or near the earth surface (ships, parked aircraft, communication centers, etc.) which are exposed to a high altitude EMP. In this case the earth surface (soil or water) gives an essential contribution to the interaction of the incident EMP with the system. One can think of this case by defining the incident EMP fields as approximately the sum of two plane waves, including the wave reflected from the (approximate) lossy half space. It is this double plane wave which is needed for testing systems on the earth surface. Fortunately, one type of EMP simulator addresses this problem reasonably well. This hybrid type of EMP simulator is somewhat more complex theoretically and combines far- and near-field considerations in a special way. While not as efficient as a parallel-plate type of simulator (in terms of, say, early-time electric field per unit pulser volt) it can achieve this special kind of double-plane-wave field distribution.

II. Equivalent-Electric-Dipole EMP Simulators

Much is now known concerning the use of electric dipoles to radiate transient electromagnetic fields with attention to both time- and frequency-domain aspects. This is briefly summarized in [15 section 2A] which also gives an extensive list of references. Here we discuss some of the principal design aspects.

The first and most important design consideration concerns the low-frequency content of the radiated pulse. It is an elementary and well-known result of antenna theory that at zero frequency an antenna cannot radiate (or cannot have a non-zero coefficient of the $1/r$ term at large distances) with appropriate practical limitations on the sources driving the antenna. For typical antenna dimensions (of, say, tens of meters) the wavelength becomes large compared to the antenna in the low MHz region and below. However, the high-altitude EMP environment does not roll off as frequency is decreased in this region [18]. Our problem is then to do the best we can in minimizing this inherent low-frequency deficiency.

A set of sources in free space enclosed in a sphere of radius r_0 gives electromagnetic fields for $r > r_0$ which can be expanded in multipole terms. At low frequencies ($\lambda \gg r_0$) the dipole terms (electric and magnetic) normally dominate the far fields ($r \rightarrow \infty$) unless these terms are suppressed (such as by the inclusion of special symmetries in the antenna design). It is then one or more dipole terms which need to be maximized. For the present discussion we consider the electric dipole term. This term gives the far field [3,10]

$$\tilde{\mathbf{E}}_f(\vec{r},s) \rightarrow -\frac{\mu_0}{4\pi} e^{-\frac{sr}{c}} \frac{s^2}{r} \hat{\mathbf{T}}_t \cdot \tilde{\mathbf{p}}(s) \quad \text{as } s \rightarrow 0$$

(2.1)

$s \equiv$ Laplace transform variable or complex frequency

$\hat{\mathbf{T}}_t \equiv \hat{\mathbf{T}} - \hat{\mathbf{i}}_r \hat{\mathbf{i}}_r \equiv$ transverse dyad

$\hat{\mathbf{i}}_r \equiv$ unit vector in the r direction in a spherical coordinate system
(r, θ, ϕ) centered on the simulator

where

$$\tilde{\mathbf{E}}(\vec{r},s) \rightarrow \tilde{\mathbf{E}}_f(\vec{r},s) \quad \text{as } r \rightarrow \infty \quad (2.2)$$

Figure 2.1 gives the coordinates for this discussion.

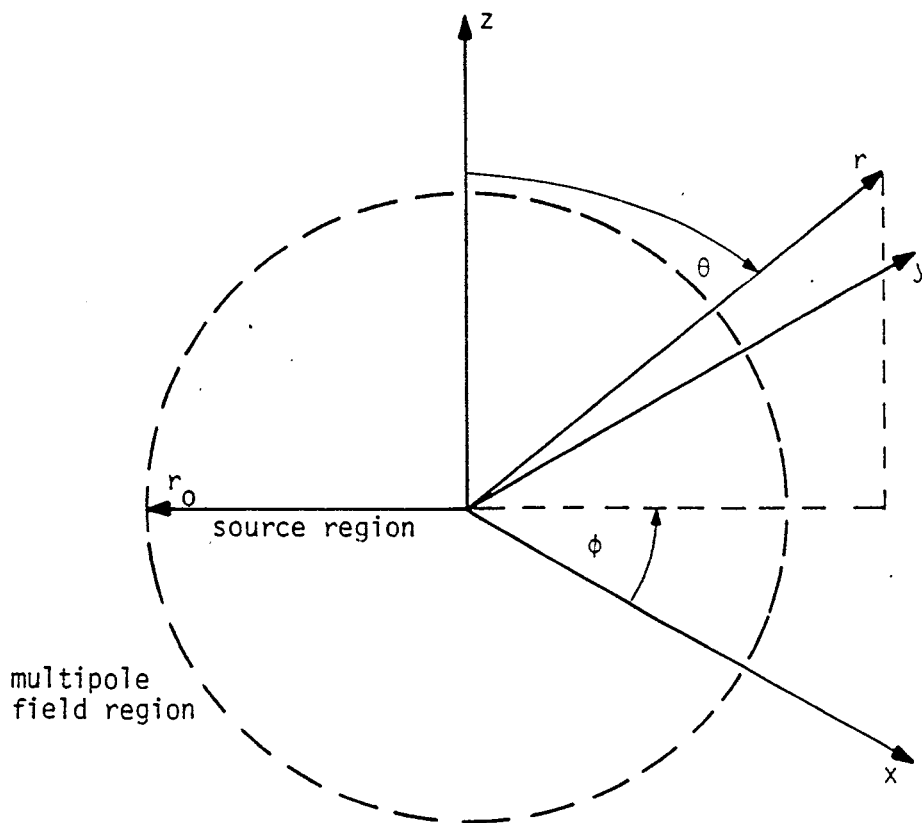


Fig. 2.1. Coordinates for Radiating Simulator

For the far fields the limited low-frequency behavior (compared to EMP) makes the low-frequency performance of primary concern. To maximize the low-frequency far simulator fields (2.1) indicates that one should maximize $\vec{p}(s)$ as $s \rightarrow 0$. It is quite possible to have

$$\vec{p}(s) \rightarrow \frac{1}{s} \vec{p}(\infty) \quad \text{as } s \rightarrow 0, \vec{p}(\infty) \neq \vec{0} \quad (2.3)$$

within the limits of finite energy in a capacitive pulser [10]. Here

$$\vec{p}(\infty) = \lim_{t \rightarrow \infty} \vec{p}(t) \quad (2.4)$$

where of course t is actually taken as some time much greater than times of concern for the simulator output.

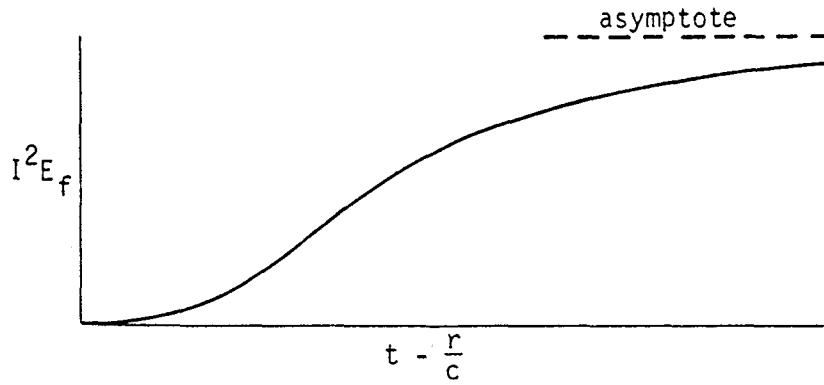
In time domain this concept of a non-zero $\vec{p}(\infty)$ has implications for the radiated (far-field) temporal waveform. As shown in [3] this property allows the radiated temporal waveform to have one zero-crossing instead of the minimum of two zero crossings required if $\vec{p}(\infty) = \vec{0}$. To illustrate this consider the example in fig. 2.2. Here powers of I indicate repeated integrals with respect to time and correspond to repeated multiplications by $1/s$ in complex-frequency domain. Noting that

$$\vec{E}_f(\vec{r}, s) \rightarrow -\frac{s\mu_0}{4\pi} \frac{e^{-sr/c}}{r} \vec{1}_t \cdot \vec{p}(\infty) \quad \text{as } s \rightarrow 0 \quad (2.5)$$

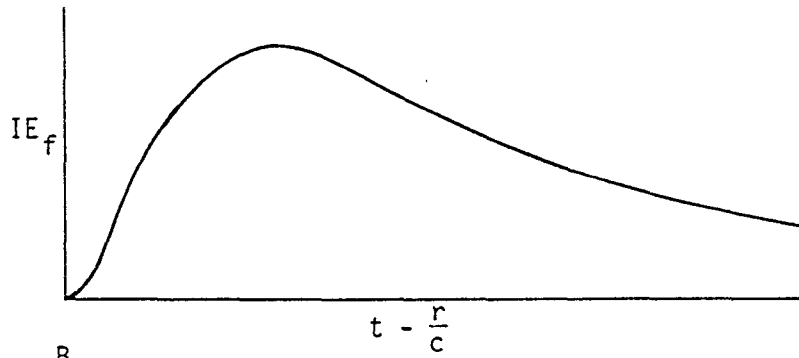
then multiplication by s^{-2} gives $I^2 E_f$ in time domain of the general form in fig. 2.2A which rises smoothly (by our choice) from zero to a late-time value governed by $\vec{p}(\infty)$ (per the Tauberian theorems of the Laplace transform). Successive differentiation gives no zero crossing in fig. 2.2B and one zero crossing in fig. 2.2C, the minimum number of zero crossings for the radiated field. If the waveform in fig. 2.2A were allowed to go back to zero then at least two zero crossings would appear in the radiated waveform. Here $\vec{p}(t)$ has been assumed to have a time-independent direction.

Note that the late-time dipole moment is computed from

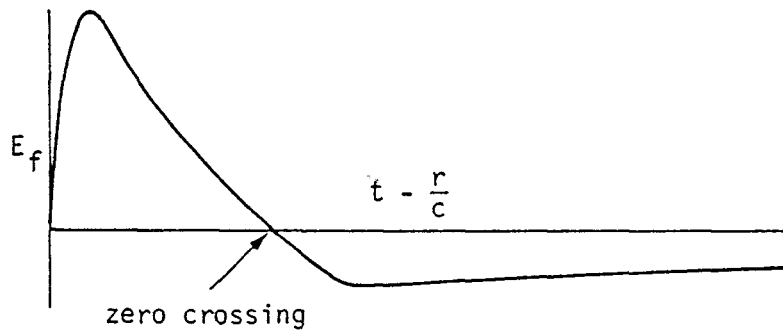
$$\vec{p}(\infty) = \int_{V'} \vec{r}' \rho_\infty(\vec{r}') dV' \equiv Q_\infty \vec{h}_{eq}$$



A.



B.



C.

Fig. 2.2. Influence of Late-Time Electric-Dipole Moment on Radiated Waveform for $\vec{p}(\infty) \neq \vec{0}$

$$\begin{aligned}
Q_\infty &= C_a V_\infty = \text{late-time charge on simulator} \\
\vec{h}_{eq} &= \text{equivalent length or mean charge separation distance} \\
\rho_\infty(\vec{r}') &= \text{late-time charge density} \\
C_a &= \text{simulator capacitance} \\
V_\infty &= V_0 \left[1 + \frac{C_a}{C_g} \right]^{-1} = \text{late time voltage on simulator} \\
V_0 &= \text{charge voltage (if Marx generator then when fully erected)} \\
&\quad \text{of capacitive pulser} \\
C_g &= \text{pulser capacitance (if Marx generator then when fully erected)}
\end{aligned}
\tag{2.6}$$

Combining these gives

$$\vec{p}(\infty) = V_0 C_a \left[1 + \frac{C_a}{C_g} \right]^{-1} \vec{h}_{eq}
\tag{2.7}$$

From this we can see how to maximize $\vec{p}(\infty)$. Note that \vec{h}_{eq} is proportional to the antenna length and C_a is proportional to the antenna length and width (or fatness, but logarithmically in the latter case). Clearly antenna length or height is a matter of primary concern. The pulse generator can also help by large V_0 and large C_g , although increasing C_g too much beyond C_a is not useful.

Having first considered the design constraints for optimum low-frequency performance let us turn to the high-frequency aspects of the design, noting that the latter should not be chosen in a form which significantly degrades the former. Fortunately a circular conical geometry is appropriate to this task. As illustrated in fig. 2.3 we have the general concept of a typical equivalent electric dipole. Note that this type of structure is analyzable by image theory. The equivalent dipole moment (for producing fields in the upper half space) includes the image in its definition; the equivalent voltage is twice the actual voltage on the cone and the equivalent capacitance is half the actual capacitance. Note that a cone has the property of being "fat" at the furthest distance from the ground plane, thereby enhancing the equivalent height. The equivalent height is further enhanced by including a top cap on the cone (of physical height h). The capacitance is enhanced by making the cone fat (i.e., a "large" value of θ_0).

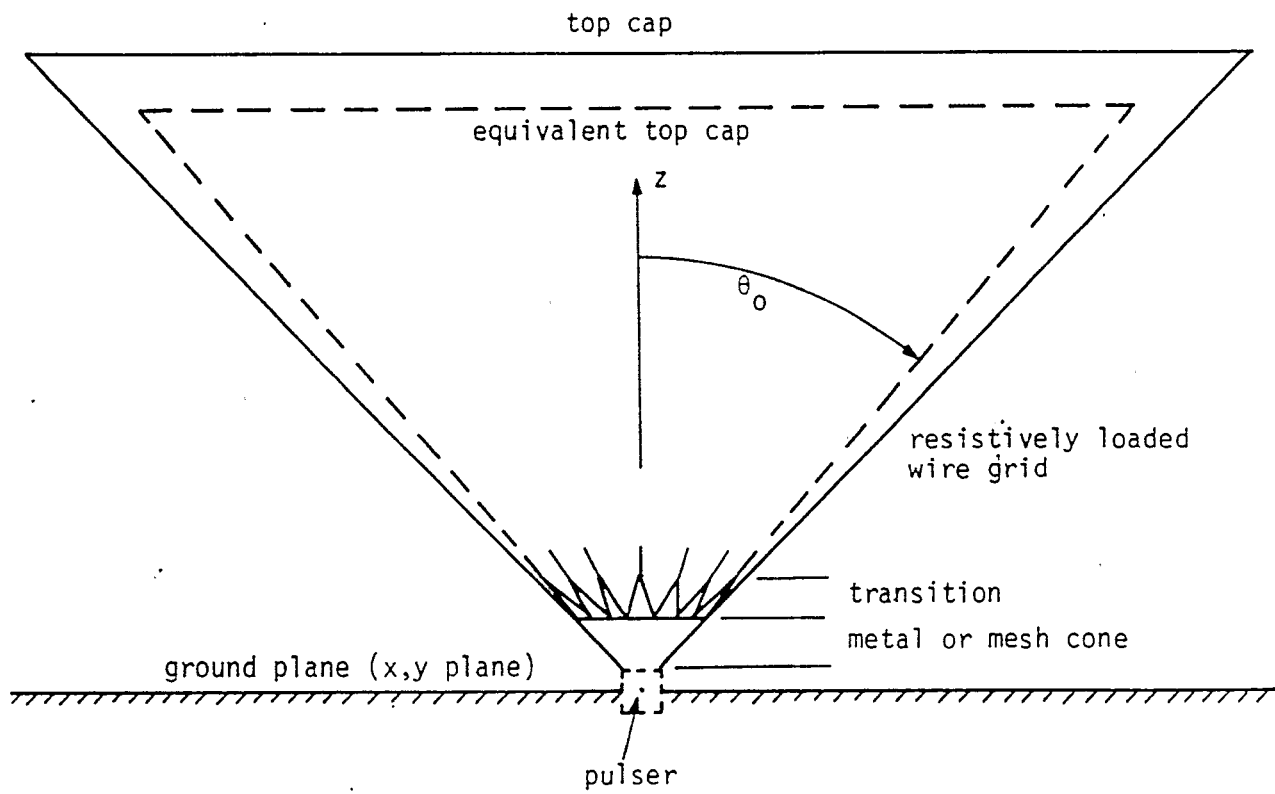


Fig. 2.3. Conical Equivalent-Electric-Dipole Simulator

Near the cone apex some care is taken to make the geometry a good approximation to a metal cone. At early times (or high frequencies) the impedance is [2,4,5]

$$\begin{aligned}
 Z_{eq} &= 2Z_a \approx Z_o f_g = Z_\infty \\
 f_g &= \frac{1}{\pi} \ln \left[\cot \left(\frac{\theta_o}{2} \right) \right] \\
 Z_o &= \sqrt{\frac{\mu_o}{\epsilon_o}} \quad (\text{wave impedance}) \\
 Z_a &\equiv \text{antenna impedance}
 \end{aligned} \tag{2.8}$$

Typical values of Z_a are 60 Ω or 75 Ω . The corresponding early-time fields are

$$\begin{aligned}
 E_\theta(t - \frac{r}{c}) &= V_{eq}(t) \left\{ 2r \sin(\theta) \ln \left[\cot \left(\frac{\theta_o}{2} \right) \right] \right\}^{-1} \\
 &= \frac{V_{eq}(t)}{2\pi r f_g} \quad \text{for } \theta_o < \theta < \pi/2
 \end{aligned} \tag{2.9}$$

$$V_{eq}(t) = 2V_a(t)$$

$$V_a(t) \equiv \text{antenna voltage}$$

These results are determined primarily by the simulator geometry near the cone apex where one should be careful to maintain the cone geometry to a high degree of approximation to support the ideal high-frequency behavior.

For intermediate frequencies or times (wavelengths of the order of the antenna height h) the antenna should be damped so as to make the radiated field non resonant (natural frequencies for $s \neq 0$ have $\text{Re}[s] \ll -|\text{Im}[s]|$) creating a smooth spectrum for $s = j\omega$. This can be accomplished quite well by use of a resistive loading on the antenna [5]

$$\begin{aligned}
 R'(\xi) &= \frac{Z_\infty}{h'} \left[1 - \frac{\xi}{h'} \right]^{-1} \\
 &= \text{resistance per unit length along antenna}
 \end{aligned} \tag{2.10}$$

ξ = arc parameter (meters) measured from cone apex along antenna "surface"

h' \equiv slant length of antenna, perhaps including radius of "top cap"

This gives an input impedance

$$\begin{aligned}\tilde{Z}_{eq}(s) &= 2\tilde{Z}_a(s) = \frac{1}{sC_{a_{eq}}} + Z_\infty = Z_\infty \left[\frac{1}{s_{h'}} + 1 \right] \\ s_{h'} &\equiv st_{h'} \\ t_{h'} &\equiv Z_\infty C_{a_{eq}} = Z_\infty \frac{C_a}{2} \\ C_a &\equiv \text{antenna capacitance}\end{aligned}\tag{2.11}$$

which is conveniently just the series combination of a resistance and a capacitance.

Including an equivalent generator capacitance and initial voltage

$$\begin{aligned}C_{g_{eq}} &= \frac{1}{2} C_g \\ V_{o_{eq}} &= 2V_o\end{aligned}\tag{2.12}$$

the radiated far-field waveform can be calculated to give [5]

$$\begin{aligned}\xi'(\theta, t) &= \frac{\sin(\theta)}{2} \left\{ \left[\frac{e^{-\alpha\tau_{h'}}}{1 - \cos(\theta)} - \frac{1 - e^{-\alpha\tau_{h'}}}{\alpha[1 - \cos(\theta)]^2} \right] u(\tau_{h'}) \right. \\ &\quad + \frac{1}{\alpha} \frac{1 - e^{-\alpha[\tau_{h'} - [1 - \cos(\theta)]]}}{[1 - \cos(\theta)]^2} u(\tau_{h'} - [1 - \cos(\theta)]) \\ &\quad + \left[\frac{e^{-\alpha\tau_{h'}}}{1 + \cos(\theta)} - \frac{1 - e^{-\alpha\tau_{h'}}}{[1 + \cos(\theta)]^2} \right] u(\tau_{h'}) \\ &\quad \left. + \frac{1}{\alpha} \frac{1 - e^{-\alpha[\tau_{h'} - [1 + \cos(\theta)]]}}{[1 + \cos(\theta)]^2} u(\tau_{h'} - [1 + \cos(\theta)]) \right\} \\ \alpha &= 1 + \frac{C_a}{C_g} = 1 + \frac{C_{a_{eq}}}{C_{g_{eq}}}\end{aligned}\tag{2.13}$$

$$\tau_{h'} = \frac{ct - r}{h'} \quad (\text{retarded time at observer})$$

$$E_{f\theta}(\theta, t) = \frac{V_0 e g}{2\pi r f_g} \xi'(\theta, t)$$

which is approximately depicted in fig. 2.2C. The zero crossing is at about $ct/h' \approx 0.7$ and there is about 20% or so undershoot, both depending on the choice of α , say between 1 and 2.

In frequency domain we have the spectrum of the far field as

$$\begin{aligned} \tilde{\xi}'(\theta, s) = \frac{\sin(\theta)}{2(s_{h'} + \alpha)} & \left\{ \frac{1}{1 - \cos(\theta)} \left[\frac{e^{-s_{h'}[1-\cos(\theta)]}}{s_{h'}[1 - \cos(\theta)]} - 1 + 1 \right] \right. \\ & \left. + \frac{1}{1 + \cos(\theta)} \left[\frac{e^{-s_{h'}[1+\cos(\theta)]}}{s_{h'}[1 + \cos(\theta)]} - 1 + 1 \right] \right\} \end{aligned} \quad (2.14)$$

$$s_{h'} = \frac{sh'}{c}$$

$$\tilde{E}_{f\theta}(\theta, s) = \frac{V_0 e g}{2\pi r f_g} \frac{h'}{c} e^{-\frac{sr}{c}} \xi'(\theta, s)$$

This spectrum varies smoothly with frequency and has asymptotic forms for high and low frequencies as

$$\tilde{\xi}'(\theta, s) \sim \frac{1}{s_{h'} \sin(\theta)} \quad \text{as } s_{h'} \rightarrow \infty \quad \text{with } \text{Re}[s_{h'}] \geq 0 \quad (2.15)$$

$$\tilde{\xi}'(\theta, s) \sim \frac{s_{h'}}{2\alpha} \sin(\theta) \quad \text{as } s_{h'} \rightarrow 0$$

As one might expect the spectrum peaks where $s_{h'}$ is of the order of 1. Note that while at low frequencies the far fields are of a dipole form, at high frequencies the far fields are very unlike a dipole. Note that the high-frequency results only apply for θ away from the axis because of shadowing by the cone (i.e., $\theta_0 < \theta < \pi/2$).

These results for the far field can be extended to give the near-field electric-dipole terms. These corrections are significant at low frequencies but apply only for $r \gg h$. The formulas for the dipole-corrected fields for $r \gg h$ are of significantly greater complexity than (2.13) and can be found in

[14]. For $r \gg h$ estimates of E_{θ} and H_{ϕ} can be obtained from transmission-line approximations for the voltage and current along the cone using the results of [5]. Note that at sufficiently early time (2.13) must be corrected to give a non-zero rise time associated with the characteristics of the pulse generator. This rise is often modelled by an inductance (switch inductance) in series with the high-frequency antenna impedance $Z_{\infty}/2$. In frequency domain (2.14) can be corrected at sufficiently high frequencies to account for the same phenomenon.

In the practical realization of a large EMP simulator of this type there are introduced design features for reducing cost, weight, and wind loading. One needs to be careful to preserve electromagnetic performance. In particular, it is desirable to replace the ideal continuously resistively loaded circular cone (and top cap) by a grid of wires with typically a set of lumped resistors. The resulting wire grid or cage can be approximately treated by considering a position for an equivalent conducting sheet (circular cone and top cap) which is "behind" (away from the external fields) a distance of the rough order of the wire spacing [1,4,11,16,17]. This implies that the wire cage should be placed outside the ideal cone on $\theta = \theta_0$ to some $\theta > \theta_0$ as indicated in fig. 2.3.

One also should pay some attention to the transition from the metal cone leaving the pulser to the wire cage structure. As indicated in fig. 2.3 one can use triangular tapers of metal sheet or mesh to accomplish this purpose. By making the length of this transition of the order of the local wire spacing in the subsequent grid one can reduce any high-frequency (or early-time) reflections of the wave propagation from the pulser along the metal (or dense-mesh) cone to the sparse wire-grid cone [16].

III. Hybrid EMP Simulator

There is a general class of EMP simulators which are by nature hybrids, combining several electromagnetic concepts. These are defined by the following three characteristics [15 section 2D].

"1) The early-time (high-frequency) portion of the waveform reaching the system is radiated from a relatively small source region compared to the major simulator dimensions.

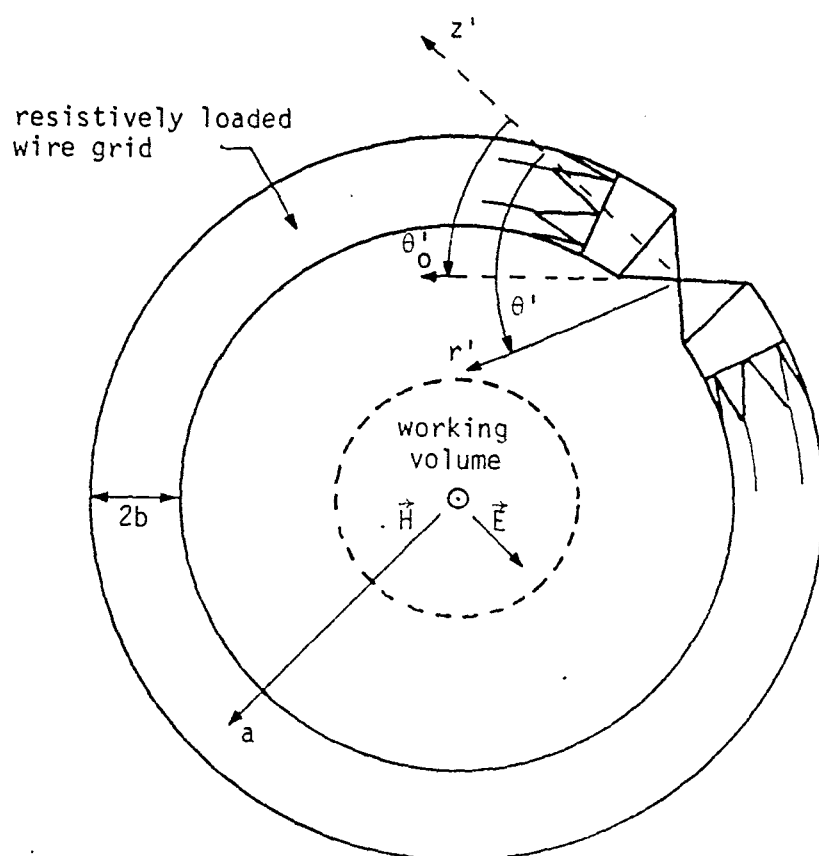
2) The low-frequency portions of the waveform are associated with currents and charges distributed over the major dimensions of the simulator structure. This structure either surrounds the system or is very close to it.

3) The structure is sparse so that most of the high-frequency energy radiates out of the simulator without reflecting off the simulator structure. The structure is also impedance loaded (including resistance) to further reduce unwanted reflections in the simulator. This also dampens oscillations in the intermediate frequency region where the simulator dimensions are comparable to an appropriate fraction of a wavelength. At low frequencies the structure reflection should become larger smoothly to make the fields transition over to the static field distribution smoothly."

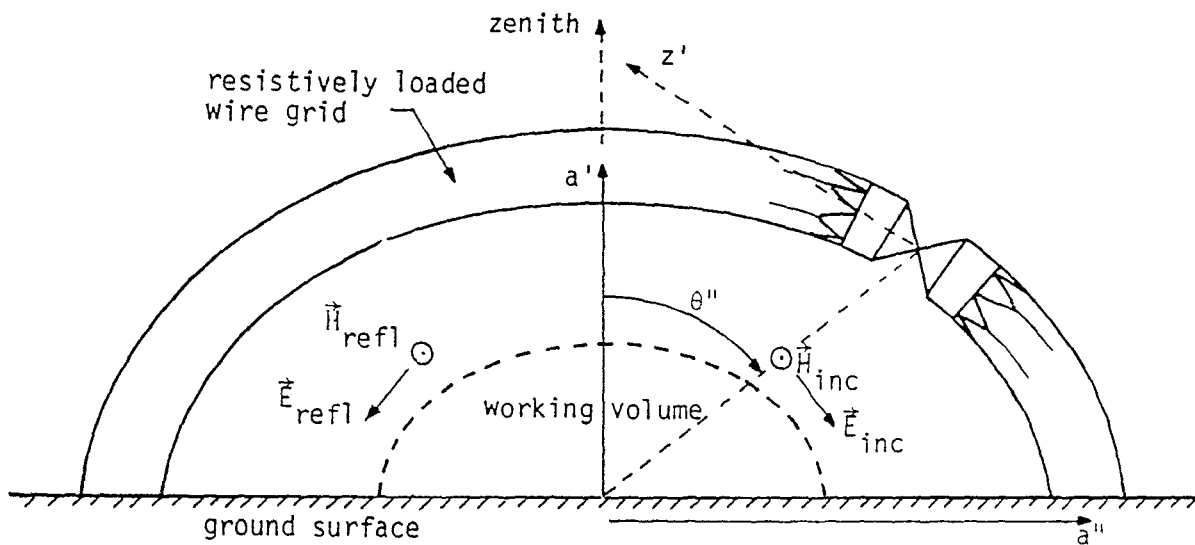
Thus a hybrid simulator is in general rather complex electromagnetically. The fields of concern are not described by a simple formula characteristic of, say an electric or magnetic dipole, which contradicts these conditions [19].

Figure 3.1 illustrates the general concept of a hybrid EMP simulator. In fig. 3.1A there is a full loop, while in fig. 3.1B there is a half loop connected to the earth (or sea water, etc.) surface. While a "full" hybrid is not typically used (to generate an approximate single plane wave) because of its relative inefficiency (field over the central working volume per pulser volt) as compared with a parallel-plate type of simulator, it is useful for understanding the performance characteristics of both kinds of hybrids. A "half" hybrid which purposefully includes the ground-reflected wave in the design can be approximately related to the "full" hybrid by image theory, including images of both the antenna and pulser.

The early-time (and generally high-frequency) behavior is controlled by the pulser and those portions of the simulator proper in the immediate vicinity



A. Full loop geometry (for single plane wave)



b. Half loop connected to earth surface (for incident plus ground-reflected plane wave)

Fig. 3.1. Hybrid EMP Simulator

of the pulser as can be seen from speed-of-light considerations. Typically, the pulser is configured to lie inside one or both cones of a circular bicone so as to launch a spherical wave on the bicone from near its apex. As such some of the results of the previous section are also applicable here in terms of the "equivalent" parameters (subscript "eq") because of the full bicone. As in fig. 3.1, using primed coordinates centered on the bicone with the z' axis as the bicone axis we have

$$Z_a \approx Z_\infty = Z_0 f_g$$

$$E_{\theta'}(t - \frac{r'}{2}) = \frac{V_a(t)}{2\pi r' f_g} \quad \text{for } \theta'_0 < \theta' < \pi - \theta'_0 \quad (3.1)$$

$$f_g = \frac{1}{\pi} \ln \cot\left(\frac{\theta'_0}{2}\right)$$

This result is limited by what is referred to as "clear time" which is the time between the first arrival of the wave from the cone apex and the arrival of the wave from the first discontinuity where the bicone is truncated and a transition to the remainder of the simulator proper (typically a resistively loaded wire cage) is begun [2]. Note that the maximum clear time is along $\theta' = \pi/2$, and that the clear time diminishes to zero at $\theta' = \theta'_0$ and $\theta' = \pi - \theta'_0$. In particular the clear time should be larger than the rise time of the waveform applied by the pulser to the bicone apex if one wishes to radiate the "peak" of the waveform before encountering the clear-time limitation. This advantage in having a large clear time also helps the high-frequency content of the resulting waveform.

This transition is similar to that discussed in the previous section except that the transition leads to a cylindrical wire cage instead of an approximate conical one. In this case the metal sheet or dense mesh cones can first transition to circular cylinders (of similar material) of a length of the order of the cone radius at the transition. This is followed by triangular tapers of a similar length leading to the wires of the cage. This transition is important so that large reflections are avoided or minimized at the discontinuity in the direction and density (sheet versus wire cage) of the simulator conductors. This is especially helpful at the higher frequencies. Note that

the effective radius of the wire cage (as an equivalent cylinder) can be computed from [4] as

$$\frac{b_{eq}}{b_1} \approx \left(\frac{Nr_0}{b_1} \right)^{1/N} \quad (3.2)$$

N \equiv number of wires in cage

b_1 = cage radius

b_{eq} = equivalent cylinder radius

r_0 = wire radius

Cross-connecting conductors (hoops) are typically used to keep the local potential differences between the wires minimal. Resonances are avoided in the resulting loops by the presence of series resistors in the wires which also give the desired resistive loading in the simulator proper.

Turning to the low frequencies ($\lambda \gg a$) let us distinguish the two cases of hybrids by a superscript "1" for the full loop giving an approximate single plane wave as in fig. 3.1A, and by a superscript "2" for the half loop connected to the earth surface giving two approximate plane waves as in fig. 3.1B. While at high frequencies the two waves are quite separable due to transit times making (3.1) applicable to both types of hybrids, at low frequencies a measurement of the electromagnetic fields of necessity includes all waves present.

Consider first the low-frequency magnetic field. In the full loop geometry of fig. 3.1A let the loop be circular (a toroid) with major radius a and minor radius b . Then relating the low-frequency magnetic field in the center to the low-frequency current by [6,8,9]

$$\tilde{H}^{(1)}(0) = \frac{\tilde{I}(0)}{2a} = \frac{Q_g}{2a} = \frac{V_0 C_g}{2a}$$

V_0 = open circuit voltage of capacitive generator
(charge voltage)

Q_g = generator charge

(3.3)

This low frequency magnetic field has the relation to the time domain waveform as its integral or "area", i.e.,

$$\tilde{H}^{(1)}(0) = \int_{-\infty}^{\infty} H(t) dt \quad (3.4)$$

Given some specified waveform then the required generator charge can be computed. If V_0 is known (say specified from (3.1)) then C_g is also determined.

For the half loop connected to the ground surface, however, we have

$$\tilde{H}^{(2)}(0) = 2 \int_{-\infty}^{\infty} H(t) dt \quad (3.5)$$

the factor of 2 accounting for the ground reflection of an incident plane wave, the reflection coefficient of the tangential magnetic field being 1.0 at low frequencies. Then using

$$\tilde{H}^{(2)}(0) = \frac{\tilde{I}(0)}{2a} = \frac{Q_g}{2a} = \frac{V_0 C_g}{2a} \quad (3.6)$$

the specification of the incident plane wave can be used to determine the generator capacitance. Note that as a practical matter the half loop is not normally circular; a good design has it made elliptical with minor radius a' and major radius a'' . This is related to the practical mechanical problem of realizing a large a' (height); a'' (half length on the ground) is much easier to make large. In this case we take

$$a \equiv \text{avg}(a', a'') \quad (3.7)$$

where the average can be of many kinds. Typically this average is chosen to make the loop area or the loop circumference the same as a loop of radius a .

Next consider the low-frequency electric field. The full loop is simpler to analyze. If the loop is resistively loaded then at low frequencies there is an electric potential (quasistatic) associated with the electric field along the loop structure given by [12,13]

$$E_{\text{tan}} = \tilde{I}(0)R' \quad (3.8)$$

R' = resistance per unit length along loop

This field establishes a potential which extends through space, in particular through the working volume in the center of the loop (simulator proper).

$$R^{(2)} = \pi a R' = \frac{Z_0}{2} \left\{ \ln\left(\frac{8a}{b}\right) - 2 \right\} \quad (3.14)$$

This half-loop resistance is typically 500Ω or a little more.

For intermediate frequencies (λ/a of the order of 1 or somewhat less) the situation is more complicated. Detailed calculations [12,13] indicate that the desired ratio of electric and magnetic fields near the center as in (3.10) is maintained typically to within about 40% or so of this ideal value across this intermediate frequency band. This shows the non-resonant character of this idealized hybrid simulator associated with radiation "losses" and resistive loading.

In transitioning from the high-frequency to a low-frequency behavior note that the impedance driven by the pulser increases significantly from that given by (3.1) (say 120Ω or 150Ω) at high frequencies to that given by (3.11) or (3.14) (say $1\text{ k}\Omega$ or 500Ω) at low frequencies. This makes the decay of the transient waveform not a simple exponential. As illustrated in fig. 3.2 the waveform initially decays rapidly but then flattens out; this is compared to a simple exponential decay with the same "area" (constrained by the pulser charge as in (3.3) or (3.6)). This example is taken for the single approximate plane wave of a full loop because of its relative simplicity. The case of two plane waves with a half loop gives a purposely more complex waveform, varying with position near the "center", which also occurs with the interference of two plane waves.

If the observer moves off the plane of the loop then other polarizations of the incident (first) plane wave become possible. On the plane of the loop the polarization is TM with respect to the vertical. However, TE polarization is achievable by placing the pulser at the top of the arch in fig. 3.1B ($\theta = 0$) and moving the observer along (or above) the ground (or near the loop axis). One should not go too far off the plane of the loop; the performance of this type of simulator is in part related to the near fields. Furthermore, TE polarization at angles of incidence near grazing to the ground significantly reduces the resultant EM fields (including ground reflection) at the observer (i.e., the system under test) thereby typically significantly reducing the interaction with the system; this is then typically a case of minimal interest.

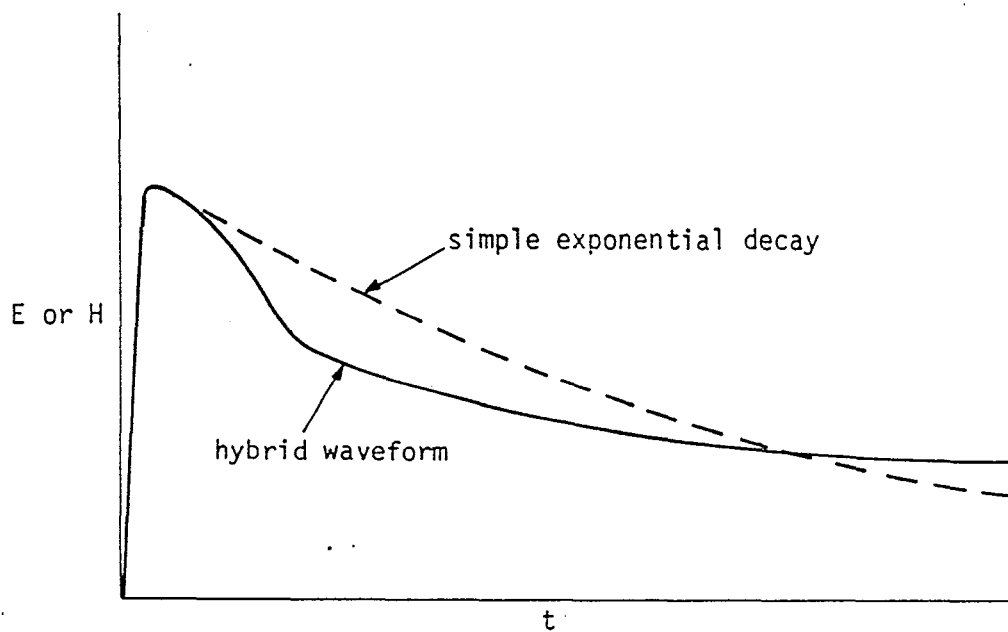


Fig. 3.2. Waveform for Ideal Hybrid in Working Volume (Case of One Plane Wave)

Circular or elliptical hybrids are not the only possible geometries, although these geometries do have some significant performance advantages. For example, another hybrid geometry has a cylinder (wire cage) divided by the pulser (effectively $\theta'' = 0$) with distant terminations from the cylinder to the ground at both ends [7]. However, beyond some point arbitrarily increasing the length of the simulator along the ground surface does not improve the fields in the working volume.

IV. Summary

These two important types of high-altitude EMP simulators are becoming widely used for their appropriate simulation roles. Both have their own optimization conditions and trade-offs which should be considered in designing such simulators for specific intended applications.

References

1. C. E. Baum, Impedances and Field Distributions for Parallel Plate Transmission Line Simulators, Sensor and Simulation Note 21, June 1966.
2. C. E. Baum, A Circular Conical Antenna Simulator, Sensor and Simulation Note 36, March 1967.
3. C. E. Baum, Some Limiting Low-Frequency Characteristics of a Pulse-Radiating Antenna, Sensor and Simulation Note 65, October 1968.
4. C. E. Baum, Design of a Pulse-Radiating Dipole Antenna as Related to High-Frequency and Low-Frequency Limits, Sensor and Simulation Note 69, January 1969.
5. C. E. Baum, Resistively Loaded Radiating Dipole Based on a Transmission-Line Model for the Antenna, Sensor and Simulation Note 81, April 1969.
6. C. E. Baum, Some Considerations Concerning a Simulator with the Geometry of a Half Toroid Joined to a Ground or Water Surface, Sensor and Simulation Note 94, November 1969.
7. C. E. Baum, Some Considerations Concerning a Simulator with the Geometry of a Cylinder Parallel to and Close to a Ground or Water Surface, Sensor and Simulation Note 97, January 1970.
8. C. E. Baum, Low-Frequency Magnetic Field Distribution for a Simulator with the Geometry of a Half Toroid Joined to the Surface of a Medium with Infinite Conductivity, Sensor and Simulation Note 112, July 1970.
9. A. D. Varvatsis and M. I. Sancer, Low-Frequency Magnetic Field Distribution of a Half Toroid Simulator Joined to a Finitely Conducting Ground: Simple Ground Connections, Sensor and Simulation Note 122, February 1971.
10. C. E. Baum, Some Characteristics of Electric and Magnetic Dipole Antennas for Radiating Transient Pulses, Sensor and Simulation Note 125, January 1971.
11. D. F. Higgins, The Effects of Constructing a Conical Antenna Above a Ground Plane Out of a Number of Thin Wires, Sensor and Simulation Note 142, January 1972.
12. C. E. Baum and H. Chang, Fields at the Center of a Full Circular TORUS and a Vertically Oriented TORUS on a Perfectly Conducting Earth, Sensor and Simulation Note 160, December 1972.
13. H. Chang, Electromagnetic Fields Near the Center of TORUS, Part 1: Fields on the Plane of TORUS, Sensor and Simulation Note 181, August 1973.

14. B. K. Singaraju and C. E. Baum, A Simple Technique for Obtaining the Near Fields of Electric Dipole Antennas from Their Far Fields, Sensor and Simulation Note 213, March 1976.
15. C. E. Baum, EMP Simulators for Various Types of Nuclear EMP Environments: An Interim Categorization, Sensor and Simulation Note 240, January 1978; also as IEEE Trans. Antennas and Propagation, January 1978, pp. 35-53, and IEEE Trans. EMC, February 1978, pp. 35-53.
16. W. S. Kehrer and C. E. Baum, Electromagnetic Design Parameters for ATHAMAS II, ATHAMAS Memo 4, May 1975.
17. C. E. Baum, J. E. Partak, J. E. Swanekamp, and T. Dana, Electromagnetic Design Parameters for NAVES II, NAVES Memo 1, March 1977.
18. K.S.H. Lee (ed.), EMP Interaction: Principles, Techniques, and Reference Data, EMP Interaction 2-1, December 1980.
19. J. D. Jackson, Classical Electrodynamics, Wiley, 1962.